

Precision half-life measurement of ^{29}P

J. Long,^{1,*} M. Brodeur,¹ M. Baines,^{1,2} D. W. Bardayan,¹ F. D. Becchetti,³ D. Blankstein,¹ C. Boomershine,¹ D. P. Burdette,¹ A. M. Clark,¹ B. Frentz,¹ S. L. Henderson,¹ J. M. Kelly,¹ J. J. Kolata,¹ B. Liu,¹ K. T. Macon,¹ P. D. O'Malley,¹ A. Pardo,^{1,4} C. Seymour,¹ S. Y. Strauss,¹ and B. Vande Kolk¹

¹*Department of Physics, University of Notre Dame, Notre Dame, Indiana 46556, USA*

²*Department of Physics, University of Surrey, Guildford, GU2 7XH, United Kingdom*

³*Department of Physics, University of Michigan, Ann Arbor, Michigan 48109, USA*

⁴*Department of Physics, Londrina State University, Londrina, Postal Code 10011, 86057-970 Londrina, Parana, Brazil*



(Received 25 September 2019; published 2 January 2020)

A new precision half-life measurement of ^{29}P was conducted using the *TwinSol* β -counting station at the University of Notre Dame Nuclear Science Laboratory. The resulting value of $t_{1/2}^{\text{new}} = 4.1055(44)$ s is the most precise ^{29}P half-life measurement to date. Utilizing this measurement and reevaluating the world data leads to a new world average of $t_{1/2}^{\text{world}} = 4.1031(58)$ s, which improves the Birge ratio from 3.11 to 1.45 and is 2.3 times more precise than the previous world value. The new Cabibbo-Kobayashi-Maskawa matrix element V_{ud} for ^{29}P shifts closer into agreement with the superallowed pure Fermi value. The uncertainty in the mixed transition value of V_{ud} , however, is still dominated by the Fermi to Gamow-Teller mixing ratio ρ . Using the new world half-life and assuming the validity of the standard model, a new predicted value for ρ and its associated correlation parameters have been evaluated in order to guide future determination of ρ .

DOI: [10.1103/PhysRevC.101.015501](https://doi.org/10.1103/PhysRevC.101.015501)

I. INTRODUCTION

Despite the great success of the standard model (SM), there are currently several experimental efforts aimed at searching for physics beyond this model since it falls short in explaining many observed features, including the matter and antimatter asymmetries in the Universe. One way the SM can be probed is through precision measurements of nuclear β decays [1], which can be used to test the unitarity of the Cabibbo-Kobayashi-Maskawa quark-mixing matrix [2]. The most precise test of this unitarity is found by taking the sum of the squares of the matrix elements in the top row, (V_{ud} , V_{us} , and V_{ub}) where normalization will equal 1 if unitarity holds. Of these elements the V_{ud} and V_{us} terms are the most important with V_{ud} dominating the matrix unitarity evaluation. V_{ud} is extracted from various superallowed β decays [2], whereas V_{us} can be calculated using kaon decays [3,4] and τ decays [5]. Recent state-of-the-art lattice QCD calculations, however, result in a significantly lower value of V_{us} that, if correct, would result in a 2.2σ tension with unitarity [6].

V_{ud} can be extracted from four different types of β decays: superallowed pure Fermi transitions, superallowed mixed transitions, pion decay, and neutron decay [2]. Currently, the most precise determination of V_{ud} is evaluated using the superallowed pure Fermi β -decay transitions [2]. Although the latest evaluation leads to unitarity, recent calculations of Δ_R , the transition-independent radiative corrections result in departures of 2.3σ [7] and 3.3σ [8] from unitarity. Furthermore,

once the latest value for V_{us} is used, the breakdown can reach a critical 5σ [6]. This situation is spurring a growing interest in evaluating V_{ud} from other kinds of decays in order to confirm the superallowed pure Fermi value. Although both neutron and pion decay have the advantage that no nuclear structure corrections need to be applied, both come with steep disadvantages. The precision from neutron decay is limited given the conflicting neutron half-life values obtained from the beam [9] and bottle [10] methods. The pion β decay suffers from a very weak branch on the order of 10^{-8} rendering achieving an improved statistical precision very difficult [11,12]. Due to these limitations, superallowed mixed β decays are becoming an increasingly competitive type of decay to extract V_{ud} and test the accuracy of the pure Fermi value.

Evaluating V_{ud} from either superallowed pure Fermi transitions or mirror transitions requires measurements of the half-life, branching ratio, and Q_{EC} value [13]. Mixed mirror β -decay transitions additionally require a measurement of the Fermi to Gamow-Teller mixing ratio ρ [13] since the Gamow-Teller decay channels are not forbidden. To extract V_{ud} from the mirror transitions, the corrected statistical rate function $\mathcal{F}t^{\text{mirror}}$ should first be calculated, defined as

$$\mathcal{F}t^{\text{mirror}} \equiv f_V t (1 + \delta'_R) (1 + \delta_{NS}^V - \delta_C^V), \quad (1)$$

where f_V is the uncorrected statistical rate function of the vector interaction, t is the partial half-life of the superallowed branch, δ'_R is the nucleus-dependent radiative correction, δ_{NS}^V is the nuclear structure correction, and δ_C^V is the isospin symmetry-breaking correction. V_{ud} can then be calculated

*jlong10@nd.edu

using

$$|V_{\text{ud}}|^2 = \frac{K}{\mathcal{F}_T^{\text{mirror}} G_F^2 (1 + \Delta_R) \left(1 + \frac{f_A}{f_V} \rho^2\right)}, \quad (2)$$

where $K/(\hbar c)^6 = 2\pi^3 \hbar \ln 2 / (m_e c^2)^5 = 8120.2776(9) \times 10^{-10} \text{ GeV}^{-4} \text{ s}$, G_F is the weak-interaction constant, Δ_R is the transition-independent radiative correction, f_A is the statistical rate function for the axial-vector part of this interaction, and ρ is the Fermi to Gamow-Teller mixing ratio.

It is important to note that measuring ρ is challenging, and, as a result, it is only known for five transitions: ^{19}Ne , ^{21}Na , ^{29}P , ^{35}Ar , and ^{37}K [13]. The mixing ratio ρ can be determined by measuring one of the decay spectra correlation parameters, the β -asymmetry parameter A_β , the neutrino asymmetry parameter B_ν , and the β -neutrino angular correlation parameter $a_{\beta\nu}$ [13]. Currently, all five nuclei for which ρ has been determined yield V_{ud} values consistent with one another [13]. A recent measurement of A_β for ^{37}K at the TRINAT experiment [14] has resulted in significant improvement in the value of V_{ud} from mirror transitions. Now, the mirror decay V_{ud} value is within 1.05σ from the pure Fermi transition value.

Of the five known mixed transition isotopes from which V_{ud} can be extracted, ^{29}P is currently the least precise. Most of the uncertainty stems from the value of ρ obtained from a single low-precision β -asymmetry measurement [15]. However, among the experimental quantities entering in the determination of the $\mathcal{F}_T^{\text{mirror}}$ value, the half-life is by far the least precisely known. This is primarily due to the small number of imprecise and conflicting measurements of the ^{29}P half-life, all of which are over 35-years old. Hence, to clarify this disagreement and improve the world half-life value for a better V_{ud} determination from the superallowed mixed β decays, a precision half-life measurement of ^{29}P has been performed at the Nuclear Science Laboratory (NSL) of the University of Notre Dame.

II. EXPERIMENTAL METHOD

For the lifetime measurement, a radioactive ion beam (RIB) of ^{29}P has been produced and separated using the twin solenoid facility *TwinSol* at the NSL. First, a stable primary beam of ^{28}Si was generated using a silicon cathode in a cesium sputtering ion source and accelerated using a FN tandem accelerator set to a terminal voltage of 9 MV. In the tandem, the negatively charged ions are accelerated toward a thin carbon stripper foil placed at the center of the tandem which removes multiple electrons. Following the accelerator, a dipole magnet separated the charge states and only selected the $^{28}\text{Si}^{8+}$ ions, which were sent to a deuterium gas target with 4- μm -thick titanium windows for RIB production.

Following its production, the ^{29}P beam was separated from the primary beam using the *TwinSol* facility. The beam of ^{29}P was then implanted on a 0.25-mm-thick gold foil placed at the NSL β -decay counting station [16,17]. The measurement was performed using the same procedure outlined in Refs. [17–19]. An electrostatic steerer plate upstream from

the FN tandem deflected the beam during counting periods to avoid additional background.

The ^{29}P half-life measurement composed of a series of implantation and counting cycles of which the majority consisted of 31 standard runs with an additional three long counting runs used to probe for longer-lived contamination. The standard runs typically consisted of 50 cycles each with a counting period of 160 s (39 half-lives), whereas the long runs typically consisted of 14 cycles each with a counting period of 650 s (159 half-lives). For each of the runs, a single parameter was varied including the photomultiplier tube bias, the discriminator threshold, or beam implantation time to probe for possible systematic effects that would affect the measurement.

III. DATA ANALYSIS

Data analysis followed the well-established method described in detail in Ref. [20], which was also used for the precision half-life measurements of ^{17}F [17], ^{25}Al [18], ^{11}C [19], and ^{20}F [21], all conducted at the NSL *TwinSol* facility. The data analysis was performed separately by two different group members to ensure the validity of results. The data were rebinned from the original 16 000 bins to 500 bins to minimize bins without counts as they may introduce a bias into the fitting procedure. This resulted in bin widths of 320 ms for the standard runs and 1.28 s for the long runs. Specific details of the data analysis are presented below.

A. Dead time per event determination

In previous precision half-life measurements conducted at the NSL, the dead time per event was calculated directly from the measured data by taking the difference between the recorded clock time and the live time over the course of a cycle divided by the total number of events. Using this method, the resulting average dead time per event over all 1671 ^{29}P cycles is $\tau = 56.34(24) \mu\text{s}$. To provide an independent check of this value, the dead time was also measured using the well-known source pulser method [22] the week following the experiment. The dead time for this method is calculated via

$$\tau = \frac{1}{R_S} \left(1 - \sqrt{\frac{R_C - R_S}{R_P}} \right), \quad (3)$$

where R_S and R_P are the rates measured from a radioactive source alone and a pulser alone, respectively, whereas R_C is the combined rate measured from the radioactive source and the pulser together. For this measurement, a ^{90}Sr source and Stanford Research Systems Model DG535 pulser were used. A total of 12 runs, each 40-min long, were collected using this method. Each run composed a measurement of the source rate alone, the pulser rate alone, and the combined rate of the two together to probe for systematic effects. For each of these runs, the photomultiplier bias, discriminator threshold voltages, and run time were all varied. Using this method, a dead time or event of $56.47(11) \mu\text{s}$ was obtained, which shows good agreement with the value obtained from the former method. This result is compared with the clock method result in Fig. 1. The weighted average of these two results in

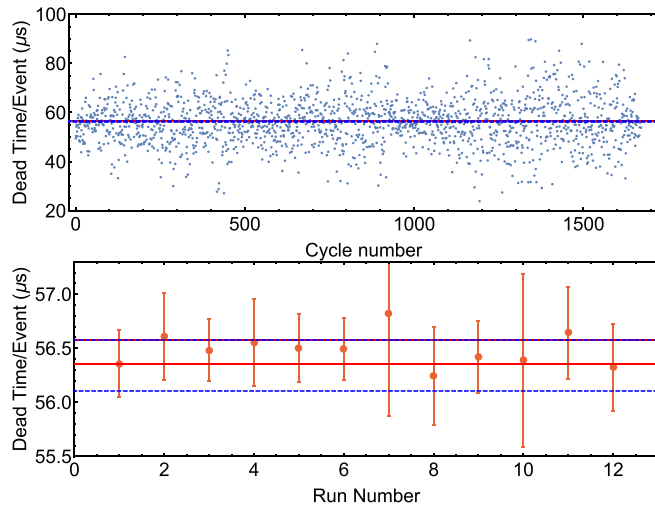


FIG. 1. Dead time per event results for the ^{29}P half-life measurement via the clock subtraction method (top panel) and the source pulser method (bottom panel). The average of the clock method data is given by the dashed blue lines. The weighted average of the source pulser method data is given by the solid red lines.

$\tau = 56.445(98) \mu\text{s}$ has been used in the analysis of the ^{29}P half-life data.

B. Half-life determination

The ^{29}P half-life has been determined using the *summed fit* method [20] where all the runs that are of the same length can be added together and treated as a single set. Hence, the 160- and 650-s long cycles were treated separately. Also, the number of counts in each bin has been corrected for losses due to the dead time inherent in the detector system using the value from Sec. III A.

The *summed fit* curve for the 31 runs with a duration of 160 s is shown in the top panel of Fig. 2. The residuals assuming only one decay component shown in the figure and the poor $\chi^2_{\nu} = 3.97$ indicate a radioactive contaminant could be affecting the half-life. To pinpoint that contaminant, a second component, with the half-life left as a floating fit variable, was added to the fit, resulting in a contaminant half-life of 6.47(22) s and contamination ratio defined as the ratio of the activity of that contaminant over the initial activity of ^{29}P of $3.35(68) \times 10^{-2}$. This matches the half-life of ^{26m}Al , 6.346 02(54) s [23], which can be produced through the exothermic $^{28}\text{Si}(d, \alpha)^{26m}\text{Al}$ reaction. When assuming an ^{26m}Al contaminant, we obtain both a better $\chi^2_{\nu} = 1.04$ and the better residuals as indicated in the bottom panel of Fig. 2.

To probe for potential long-lived contaminants, a *summed fit* of the three runs consisting of 650-s long cycles was also taken. The result assuming only an ^{26m}Al contaminant is shown in the top panel of Fig. 3. Once again, both the $\chi^2_{\nu} = 1.11$ and the presence of a structure in the residuals points to a possible longer-lived contaminant. If a second contaminant with a variable half-life is added to the ^{26m}Al contaminant, it results in an improved χ^2_{ν} value of 0.93.

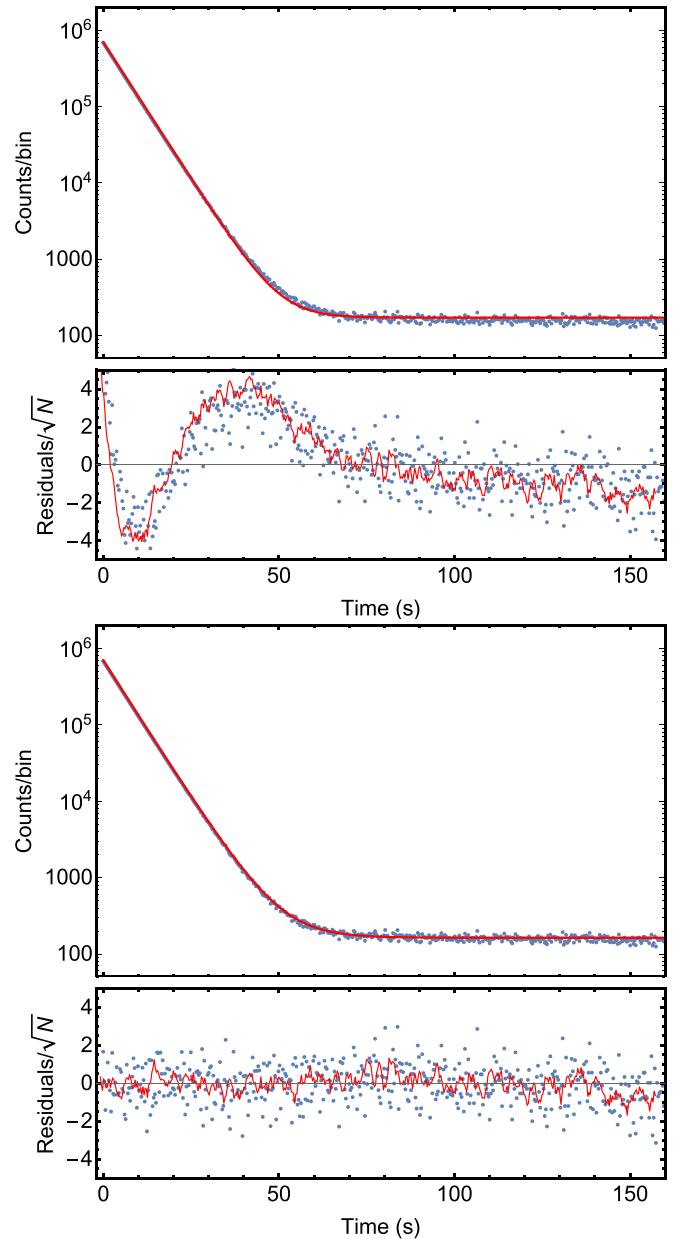


FIG. 2. Top: Summed β -decay curve of the 31 standard runs of 160 s and the residuals divided by the square root of the number of counts in each bin with strong indication of a contaminant. The red line over the residuals represents the five-point moving average. Bottom: Same as above with the inclusion of an ^{26m}Al contaminant in the fit function.

Additionally, the residuals are improved upon assuming an additional contaminant.

Another way to probe a dataset for unaccounted contaminants is to remove leading bins of the decay curve and perform the *summed fit* procedure on the remaining bins. Up to the first 15 half-lives of the 650-s decay curve were removed, corresponding to over 98% of all measured counts. If points are removed after this, there is not enough ^{29}P activity left to perform a meaningful fit for that half-life. Figure 4 compares the results assuming only an ^{26m}Al contaminant (top panel)

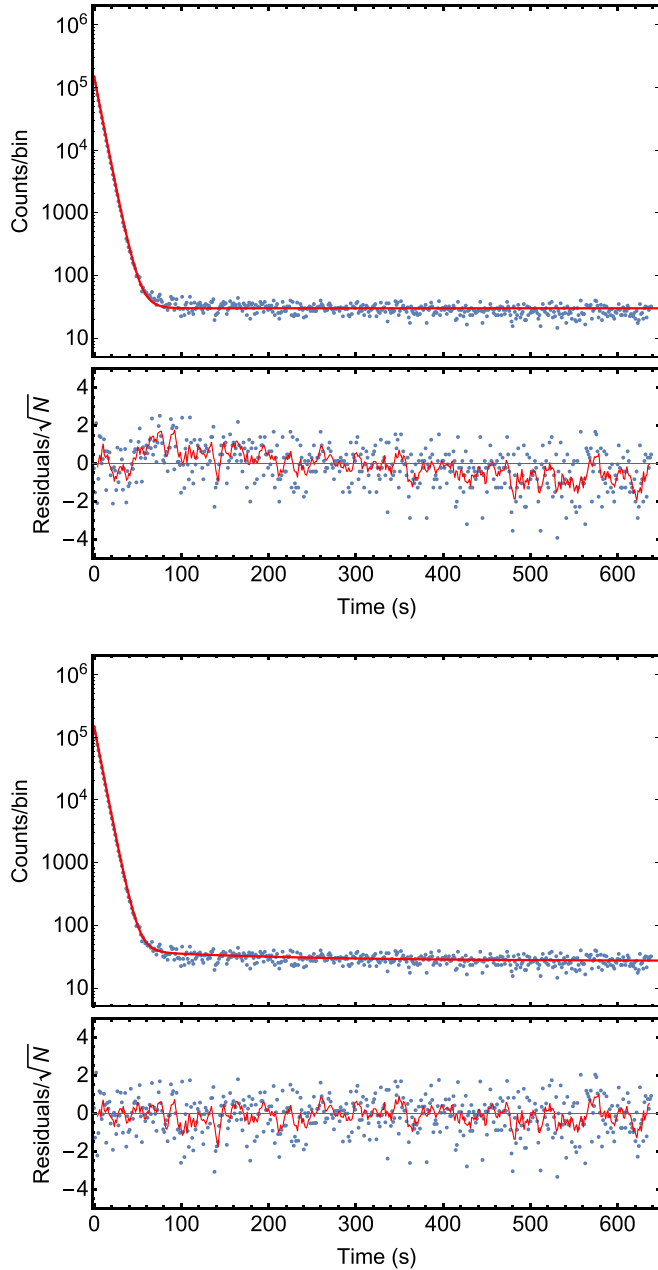


FIG. 3. Summed β -decay curve for the three 650-s long runs combined with the residuals divided by the square root of the number of counts in each bin. The red line over the residuals represents the five-point moving average. The top panel shows the fit results assuming ^{26m}Al as the only contaminant, whereas the bottom panel shows the fit result with ^{26m}Al and a second contaminant, which, in this case, is assumed to be ^{15}O .

with the ones including an additional longer-lived contaminant (bottom panel). As can be seen in the figure, the half-life for the first fit trends up to a higher value after all the ^{29}P and ^{26m}Al have decayed leaving only a residual longer-lived contaminant. Adding this third component greatly improved the fit as can be seen in comparing the fit with only ^{26m}Al in the top panel of Fig. 3 with the fit assuming an ^{15}O contamination in the bottom panel of Fig. 3.

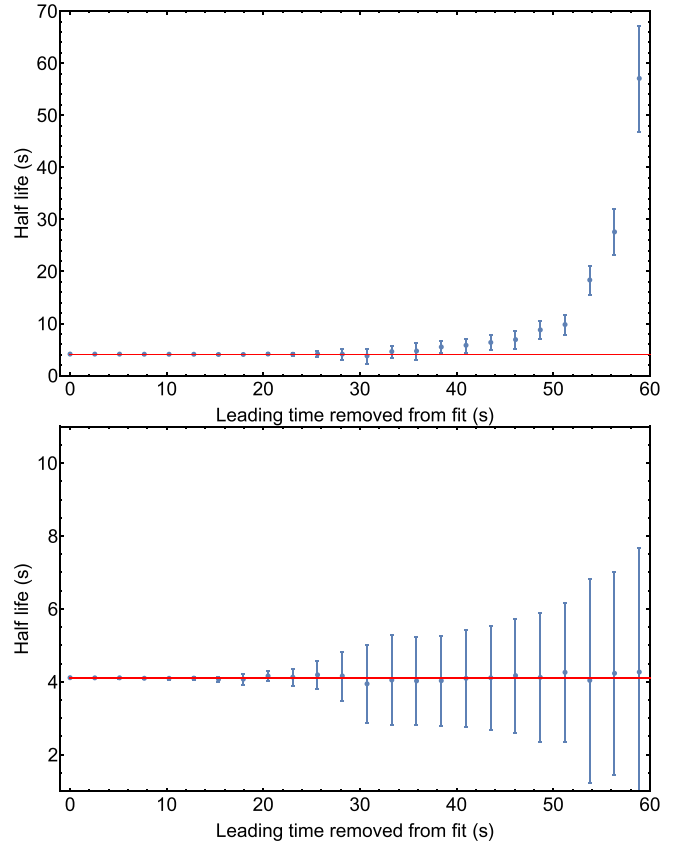


FIG. 4. Fitted half-lives for the long runs with leading bins removed and the fit performed on the remaining bins with the top panel showing the results for a fit with ^{26m}Al as the only contamination and the bottom showing the results with an additional floating contaminant. Up to 15 half-lives were removed for each, and the red lines indicate the uncertainty on the summed fit without any bin removal.

To determine this second contaminant, a fit function in the form

$$r(t) = r_0(e^{-(\ln 2)t/t_1} + R_2e^{-(\ln 2)t/t_2} + R_3e^{-(\ln 2)t/t_3}) + b \quad (4)$$

was used, where r_0 is the initial rate, t_1 is the half-life of ^{29}P , R_2 is the ^{26m}Al to the ^{29}P contamination ratio, $t_2 = 6.346\,02(54)$ s is the ^{26m}Al half-life from the literature [23], R_3 is the contamination ratio of the unknown contaminant to ^{29}P , t_3 is the half-life of this unknown contaminant, and b is the background.

The fit procedure assuming a second contaminant and a floating t_3 yielded a R_3 result of $1.09(15) \times 10^{-4}$ and $t_3 = 137(44)$ s. As performed previously, the literature was surveyed for nuclei with half-lives in the range of 137(44) s of which the possible candidates that could have been produced at *TwinSol* were ^{15}O , ^{28}Al , and ^{30}P . The various production mechanisms of these possible contaminants have been studied, and the most likely process is via transfer reactions involving the incoming ^{28}Si beam with residual air present inside the production cell or on its windows.

Nevertheless, since none of the above contaminants could be conclusively eliminated, *summed fits* were performed for

TABLE I. ^{29}P half-life assuming the different possible second contaminants. Results for the standard (160-s) and the long (650-s) runs as well as their weighted average. The bottom row gives the final ^{29}P half-life chosen. See the text for details.

Candidate	Standard (s)	Long (s)	Average (s)
^{15}O	4.1056(35)	4.105(13)	4.1056(34)
^{30}P	4.1055(35)	4.103(13)	4.1054(34)
^{28}Al	4.1056(35)	4.104(13)	4.1055(34)
Final			4.1055(34)

the standard and long runs assuming each of the three isotopes. Hence, we fixed the contamination half-life t_3 to the literature half-lives of ^{15}O , ^{28}Al , and ^{30}P which are 122.24(27) s [24], 137.70(12) s [25], and 149.88(24) s [26], respectively. The resulting ^{29}P half-lives are given in Table I. As can be seen, regardless of the assumed second contaminant, the standard and long run half-lives agree within one standard deviation. Therefore, we took a weighted average of the standard and long runs, and the results are shown in the last column of Table I. As the differences among the three half-lives obtained indicate, the determination of the second contaminant has little effect on the ^{29}P half-life. Nevertheless, to be conservative, the final ^{29}P half-life was taken as the arithmetic average of the highest and lowest ^{29}P results, and the largest uncertainty was added in quadrature to half the difference between the maximum and the minimum values. This resulted in a ^{29}P half-life value of 4.1055(34) s.

C. Uncertainty estimation

Several sources of systematic uncertainty were probed in the *summed fits* procedure using Eq. (4) and described in Sec. III B. In this procedure, t_2 is fixed at the ^{26m}Al literature half-life and t_3 fixed at the ^{15}O , ^{28}Al , and ^{30}P half-lives for three summed fits results. The average is then taken of the maximum and minimum ^{29}P half-life results and then assigned the largest uncertainty of the three. The sources of uncertainty considered here include the effects from the uncertainty in the dead time value, the number of bins chosen, the clock, the ^{26m}Al literature half-life, and in the second contaminant that has been discussed above. These results are summarized in Table II.

TABLE II. Various sources contributing to the the overall uncertainty of the ^{29}P half-life.

Source	Uncertainty (μs)
Dead time	504
Binning	334
Clock time	41
^{26m}Al half-life	23
Unknown contaminant half-life	2.9
Total systematic uncertainty	606

1. Dead time uncertainty

The uncertainty in the dead time $\tau = 56.445(98) \mu\text{s}$, presented in Sec. III A, will affect the fitted result of the ^{29}P half-life. To probe for this effect, *summed fits* over all the runs were performed with a binning of 500 and for the upper and lower values of the 1σ range in dead times $\tau = 56.543$ and $\tau = 56.347 \mu\text{s}$. The difference of the half-life from each of these fits divided by two was taken as a systematic uncertainty, contributing 0.50 ms to the overall uncertainty.

2. Time-binning choice uncertainty

The choice of binning may affect the half-life obtained. This effect was investigated by choosing different numbers of time bins: 250, 500, and 1000. This corresponds to time widths of 640, 320, and 160 ms for the standard runs and 2.56, 1.28, 0.64 s for the long runs. A lower number of bins has previously been shown to lead to a bias in the obtained half-life [18]. The largest deviation of 0.66 ms in the half-life with the 500-bin result came from using 250 bins. Half of this value, 0.33 ms, was added in quadrature to the overall uncertainty.

3. Clock time uncertainty

The clock frequency was measured using a Teledyne Lecroy 500-MHz oscilloscope to be 99.9996(10) Hz. Two additional *summed fits* with all the runs combined were performed, each with the upper and lower clock values within the limits of the uncertainty. Half the difference between the results 0.041 ms was taken as clock time uncertainty.

4. ^{26m}Al half-life uncertainty

The effect of the uncertainty in the ^{26m}Al literature half-life value of 6.346 02(54) s was also tested in the same way the clock and dead time uncertainties were probed. The highest and lowest values within uncertainty, being 6.346 56 and 6.345 48 s, were both used in the summed fit procedure yielding a half-difference in the ^{29}P half-life of 0.023 ms.

5. Unknown contaminant uncertainty

Finally, the effect of each of the candidates for the unknown contaminant was also systematically probed. The analysis was rerun with both the upper and the lower limits of literature half-lives of ^{15}O , ^{30}P , and ^{28}Al . Of these three results, the largest deviation came from the ^{15}O half-life, which yielded a change in the ^{29}P half-life value of 2.9 μs , which was then added in quadrature to the overall uncertainty.

6. Other systematic effects

To probe for additional systematic effects, the data were also subject to the *summed fit* procedure on a run-by-run basis, keeping t_2 and t_3 fixed in the same manner as described above. The fit results for the ^{29}P half-life are shown in Fig. 5 with a weighted average half-life result of 4.1045(34) s. This value is in good agreement with the fit result for the ^{29}P half-life value of 4.1055(34) s.

Other systematic effects were explored, including the influence of the photomultiplier voltage and the discriminator

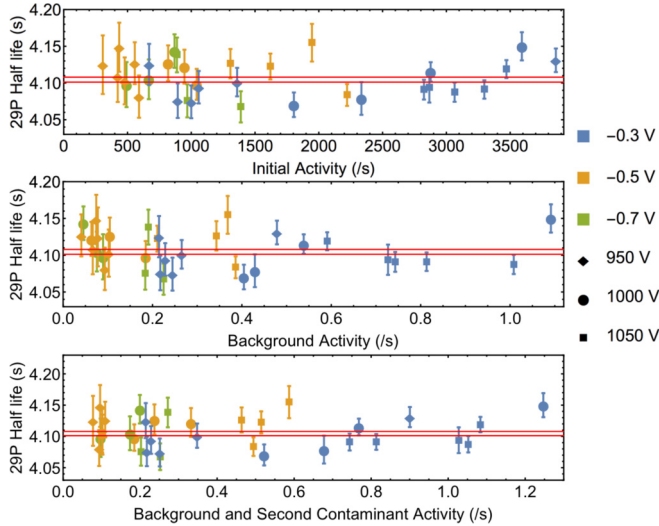


FIG. 5. Half-lives of ^{29}P vs the initial activity (top panel), the background activity (middle panel), and background activity added to the activity of the second contaminant (bottom panel) for each run. The color denotes the discriminator voltage, and the shape denotes the photomultiplier tube voltage. The final half-life result from the fitting of all the runs together 4.1055(44) s is given by solid red lines.

threshold. The photomultiplier tube was set to 950, 1000, and 1050 V and the discriminator was set to -0.3 , -0.5 , and -0.7 V. Runs combining nearly all possible combinations of both photomultiplier tube and discriminator voltages with a sufficient initial activity were taken as shown in Fig. 5. As can be seen in the figure, there are no apparent systematic changes in the half-life due to either the initial or the background activity or the sum of the background and the second contaminant activity. As Fig. 5 indicates, no systematic effects on the ^{29}P half-life with respect to the photomultiplier tube or discriminator threshold seem to be present. It should be noted that the primary beam current was not adjusted when varying either the photomultiplier or the discriminator threshold voltage. As a result, when the discriminator threshold is changed from -0.3 to -0.7 V, more low-energy β 's are being cut, which, in turn, reduces the background and observed activity. Similarly, lowering the photomultiplier voltage will reduce the gain of the photomultiplier, which will result in lower amplitude pulses, some of which will be below the discriminator threshold and not be recorded. Hence, lowering either the photomultiplier or the discriminator threshold voltage results in a decrease in the observed activity and background rates as observed in Fig. 5.

Nevertheless, all the standard runs with identical photomultiplier voltage settings and identical threshold settings were grouped together and fit using the *summed fit* procedure with the results presented in Fig. 6. The long runs were included with a weighted average, just as they were in the main fitting procedure as they cannot be folded into a *summed fit* with the standard runs due to their difference in length. As the figure indicates, all results are consistent. The weighted average for the grouping by photomultiplier voltage gives 4.1044(34) s, and the average of the runs grouped by

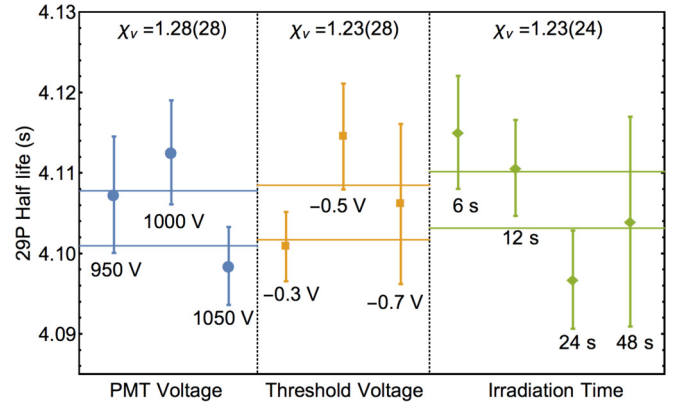


FIG. 6. Half-lives of ^{29}P when a *summed fit* is performed on all runs of identical settings according to photomultiplier voltage, threshold voltage, and irradiation time. The weighted average for each partition is given by the solid lines. The Birge ratio for each setting is given at the top of each partition.

discriminator voltage give a result of 4.1051(34) s. Both of these are consistent with the *summed fit* result of 4.1055(34) s. The Birge ratio [27] of photomultiplier voltage group is 1.28(28), and the Birge ratio for the threshold voltage group is 1.23(28). If the Birge ratio is close to 1, it implies the fluctuations in the data from run to run are statistical in nature.

In addition to the photomultiplier tube and discriminator threshold voltages, the dataset was also probed for systematic effects relating to the irradiation time of the ^{29}P RIB on the gold foil in the β counter. For the 31 standard runs, the irradiation time was varied such that there were 10 runs irradiated for 6 s, 11 runs irradiated for 12 s, and 10 runs irradiated for 24 s. The three long runs were irradiated for 48-s each. Performing a *summed fit* for each of these settings grouped together gives the result summarized in Fig. 6 where the weighted average of the four points 4.1055(34) s is given by the red lines. This value agrees well with the *summed fit* result. The Birge ratio for the dataset partitioned by irradiation time is 1.23(24).

A Birge ratio greater than one implies that the uncertainty of the weighted average analysis is slightly underestimated, possibly due to systematic effects. To correct for this, and following the Particle Data Group's [28] procedure, the uncertainty on our *summed fit* value should be inflated directly by the Birge ratio of 1.28(28), the largest of the three presented above to be conservative. Hence, the *summed fit* result from Sec. III B has been inflated by this Birge ratio, resulting in a value of 4.1055(43) s.

Adding the systematic uncertainties from the dead time, binning choice, the clock, the ^{26m}Al half-life, and the unknown second contaminant result in a total systematic uncertainty of 606 μs . When added in quadrature to the statistical uncertainty, it yields a total uncertainty of 0.0044 s giving a ^{29}P half-life of 4.1055(44) s.

IV. ^{29}P HALF-LIFE

This new precision half-life of ^{29}P is the most precise measurement to date as indicated in Fig. 7. A new world

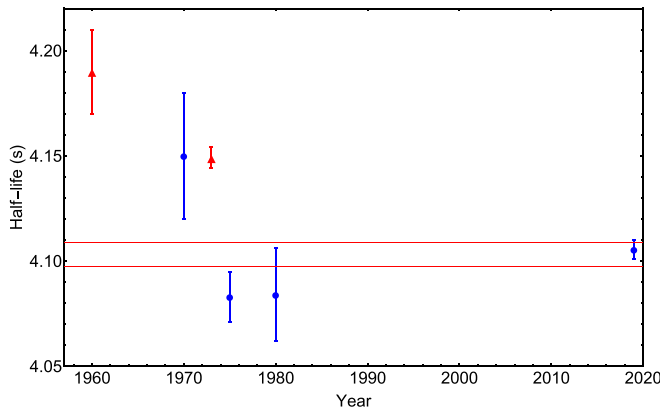


FIG. 7. ^{29}P half-lives [32–34] considered in the evaluation of the new world value. The triangle points colored red were removed from our evaluation. The scaled uncertainty on the overall ^{29}P half-life of 4.1031(58) s is represented by the red band.

value was calculated using the measurement from this paper whereas also reevaluating the measurements contributing to the previous world value. Using the same criteria as Ref. [29], two past ^{29}P half-life measurements [30,31] used in the calculation of the previous world value were rejected due to explicit use of least-squares fitting, whereas the remaining past measurements [32–34] were retained in the evaluation. The past half-lives used to find the new world value are shown in blue in Fig. 7, whereas the rejected measurements are in red. A weighted average yields a half-life of 4.1031(40) s. The Birge ratio for this average is 1.45(24), an improvement over the previous value of 3.11(21). As mentioned earlier, a Birge ratio greater than 1 implies that the uncertainty in the dataset is underestimated, and so the uncertainty from the weighted average is inflated by the Birge ratio giving a final new ^{29}P world half-life value of 4.1031(58) s. This new world average is shown by the red band in Fig. 7.

V. DISCUSSION

In order to calculate the ft value for the ^{29}P mixed transition, we combine the new ^{29}P half-life world value with the Q_{EC} value and the branching ratio. Utilizing the parametrization from Ref. [35] and the Q_{EC} value = 4942.2(4) keV from Ref. [36] results in a $f_v = 1136.33(53)$. Combining this with the branching ratio 98.290(30)%, the electron capture fraction $P_{EC} = 0.075$, the theoretical corrections $\delta'_R = 1.453(26)\%$, and $\delta'_C - \delta'_{NS} = 1.07(6)\%$ [24] yield a $\mathcal{F}t^{\text{mirror}}$ value of 4764.6(79) s. The relative uncertainties for these quantities are shown in Fig. 8. The ^{29}P half-life from this paper improves the precision on the $\mathcal{F}t^{\text{mirror}}$ value by a factor of 2.3 while decreasing it by 42.9 s. A predicted value for the mixing ratio can now be calculated using Ref. [24],

$$\mathcal{F}t^{\text{mirror}} = \frac{2\mathcal{F}t^{0^+ \rightarrow 0^+}}{1 + \frac{f_A}{f_V}\rho^2}, \quad (5)$$

where $\mathcal{F}t^{0^+ \rightarrow 0^+} = 3072.27(72)$ s [23] is the average value of the 14 most precisely known pure Fermi $0^+ \rightarrow 0^+$ superallowed transitions and f_A is the axial-vector part of the

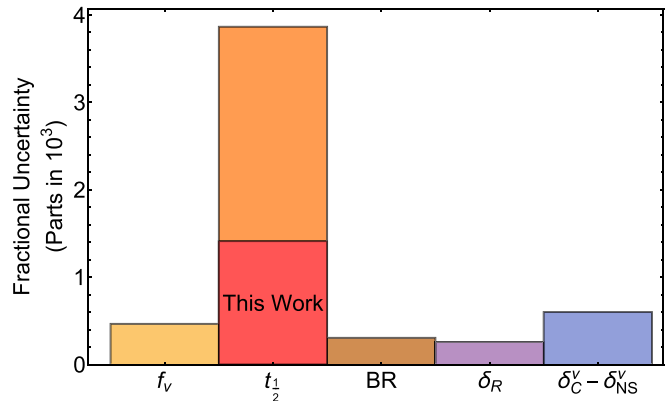


FIG. 8. The relative uncertainties for quantities needed to calculate $\mathcal{F}t^{\text{mirror}}$.

statistical rate function, which was found to be 1161.67(54) using the parametrization in Ref. [35]. The measurable parameters for ρ , a_{SM} , A_{SM} , and B_{SM} were also calculated assuming the validity of the standard model. These results are summarized in Table III.

The standard model predicted value for ρ given the new half-life measurement, Q_{EC} value, and branching ratio is $-0.5323(23)$. There is currently one measurement of ρ given in the literature, which is a β -asymmetry parameter A_β measurement [15] resulting in $A_\beta = 0.681(86)$ from which a value of $\rho = -0.593(104)$ can be derived. This value and the predicted one are within 0.6σ , meaning the current measurement stands in agreement with the standard model. The uncertainty in the ρ determination from Ref. [15] currently dominates the uncertainty in extracting V_{ud} from the ^{29}P mixed transition. Nevertheless, extracting a new V_{ud} for ^{29}P with the updated half-life using Eq. (2) gives a value of 0.949(44), shifting the value up from the previous ^{29}P value for V_{ud} of 0.945(44). It is important to note that this evaluation of V_{ud} used a value of $\Delta_R = 2.361(38)$ [37], but this V_{ud} will shift if other other values of Δ_R [7,8] are used. Combining this result with the V_{ud} values for ^{19}Ne [38], ^{21}Na [39], ^{35}Ar [13], and ^{37}K [14] leads to a value of

$$\langle V_{\text{ud}} \rangle_{\text{mirror}} = 0.9725(14). \quad (6)$$

This result is summarized in Fig. 9. Due to the large uncertainty for V_{ud} in the ^{29}P transition, which stems from the

TABLE III. Values for various parameters of relevance for determining V_{ud} from the ^{29}P mirror transition assuming the validity of the standard model.

Parameter	This paper	With previous $t_{1/2}$
$t_{1/2}$	4.1031(58) s	4.140(16) s
$f_v t$	4747.1(72) s	4790(19) s
$\mathcal{F}t^{\text{mirror}}$	4764.6(79) s	4807(19) s
ρ	$-0.5323(23)$	$-0.5216(49)$
a_{SM}	0.7056(20)	0.7148(42)
A_{SM}	0.6261(21)	0.6161(46)
B_{SM}	0.33175(16)	0.33089(44)

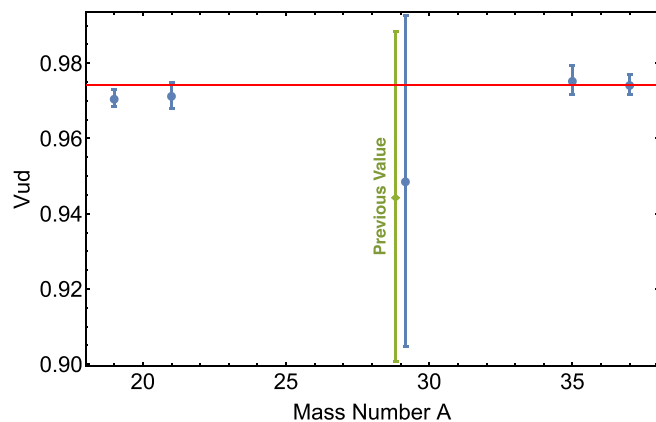


FIG. 9. Measurements of V_{ud} from the mirror β decays. The current values are given in blue circles, whereas the previous ^{29}P V_{ud} value is noted by the green diamond. The blue lines give the weighted average of the five V_{ud} values, whereas the V_{ud} value for the more precise superallowed β decays [23] are represented by the red band.

uncertainty in ρ , the small shift in the ^{29}P V_{ud} minimally affects the overall V_{ud} value combining all mirror nuclei.

VI. OUTLOOK

The most precise half-life measurement of ^{29}P to date has been performed at the NSL of the University of Notre Dame using radioactive ion beams from the *TwinSol* facility. A reevaluation of the world data, including this measurement, increases the precision of the literature value by a factor of 2.3. The largest uncertainty contributing to the f_{vt} value is still due to the half-life, so additional independent precision measurements of the ^{29}P half-life are still required. Finally, in order to improve the precision of V_{ud} extracted from the mirror decays via the ^{29}P transition, more precise measurements of the Fermi to Gamow-Teller mixing ratio ρ are needed. In order to help meet this need, a Paul trap is currently being designed and constructed for use in conjunction with the *TwinSol* facility at the NSL [40–42].

ACKNOWLEDGMENTS

We would like to acknowledge the help of N. Brodeur during this experiment. This work was supported by the National Science Foundation (NSF) Grants No. PHY-1713857, No. PHY-1401343, and No. PHY-1401242.

- [1] M. González-Alonso, O. Naviliat-Cuncic, and N. Severijns, *Prog. Part. Nucl. Phys.* **104**, 165 (2019).
- [2] J. C. Hardy and I. S. Towner, *Rep. Prog. Phys.* **73**, 046301 (2010).
- [3] M. Antonelli *et al.*, *Eur. Phys. J. C* **69**, 399 (2010).
- [4] M. Moulson, [arXiv:1704.04104](https://arxiv.org/abs/1704.04104).
- [5] E. Gámiz, [arXiv:1301.2206](https://arxiv.org/abs/1301.2206).
- [6] S. Aoki *et al.*, [arXiv:1902.08191](https://arxiv.org/abs/1902.08191).
- [7] A. Czarnecki, W. J. Marciano, and A. Sirlin, *Phys. Rev. D* **100**, 073008 (2019).
- [8] C.-Y. Seng, M. Gorchtein, H. H. Patel, and M. J. Ramsey-Musolf, *Phys. Rev. Lett.* **121**, 241804 (2018).
- [9] A. T. Yue, M. S. Dewey, D. M. Gilliam, G. L. Greene, A. B. Laptev, J. S. Nico, W. M. Snow, and F. E. Wietfeldt, *Phys. Rev. Lett.* **111**, 222501 (2013).
- [10] R. W. Pattie *et al.*, *Science* **360**, 627 (2018).
- [11] D. Počanić *et al.*, *Phys. Rev. Lett.* **93**, 181803 (2004).
- [12] N. Severijns, M. Beck, and O. Naviliat-Cuncic, *Rev. Mod. Phys.* **78**, 991 (2006).
- [13] O. Naviliat-Cuncic and N. Severijns, *Phys. Rev. Lett.* **102**, 142302 (2009).
- [14] B. Fenker *et al.*, *Phys. Rev. Lett.* **120**, 062502 (2018).
- [15] G. S. Masson and P. A. Quin, *Phys. Rev. C* **42**, 1110 (1990).
- [16] T. Ahn *et al.*, *Nucl. Instrum. Methods Phys. Res., Sect. B* **376**, 321 (2016).
- [17] M. Brodeur *et al.*, *Phys. Rev. C* **93**, 025503 (2016).
- [18] J. Long *et al.*, *Phys. Rev. C* **96**, 015502 (2017).
- [19] A. A. Valverde *et al.*, *Phys. Rev. C* **97**, 035503 (2018).
- [20] V. T. Koslowsky, E. Hagberg, J. C. Hardy, G. Savard, H. Schmeing, K. S. Sharma, and X. J. Sun, *Nucl. Instrum. Methods Phys. Res., Sect. A* **401**, 289 (1997).
- [21] D. P. Burdette *et al.*, *Phys. Rev. C* **99**, 015501 (2019).
- [22] A. P. Baerg, *Metrologia* **1**, 131 (1965).
- [23] J. C. Hardy and I. S. Towner, *Phys. Rev. C* **91**, 025501 (2015).
- [24] N. Severijns, M. Tandecki, T. Phalet, and I. S. Towner, *Phys. Rev. C* **78**, 055501 (2008).
- [25] M. Shamsuzzoha Basunia, *Nucl. Data Sheets* **114**, 1189 (2013).
- [26] M. S. Basunia, *Nucl. Data Sheets* **111**, 2331 (2010).
- [27] R. T. Birge, *Phys. Rev.* **40**, 207 (1932).
- [28] J. Beringer *et al.* (Particle Data Group), *Phys. Rev. D* **86**, 010001 (2012).
- [29] J. C. Hardy and I. S. Towner, *Phys. Rev. C* **71**, 055501 (2005).
- [30] J. Jänecke, *Z. Naturforsch., A: Astrophys., Phys. Phys. Chem.* **15**, 593 (1960).
- [31] I. Tanihata, T. Minamisono, A. Mizobuchi, and K. Sugimoto, *J. Phys. Soc. Jpn.* **34**, 848 (1973).
- [32] P. J. Scanlon and D. Crabtree, *Can. J. Phys.* **48**, 1578 (1970).
- [33] G. Azuelos and J. E. Kitching, *Phys. Rev. C* **12**, 563 (1975).
- [34] H. S. Wilson, R. W. Kavanagh, and F. M. Mann, *Phys. Rev. C* **22**, 1696 (1980).
- [35] I. S. Towner and J. C. Hardy, *Phys. Rev. C* **91**, 015501 (2015).
- [36] M. Wang, G. Audi, F. Kondev, W. Huang, S. Naimi, and X. Xu, *Chin. Phys. C* **41**, 030003 (2017).
- [37] W. J. Marciano and A. Sirlin, *Phys. Rev. Lett.* **96**, 032002 (2006).
- [38] B. M. Rebeiro *et al.*, *Phys. Rev. C* **99**, 065502 (2019).
- [39] J. Grinyer, G. F. Grinyer, M. Babo, H. Bouzomita, P. Chauveau, P. Delahaye, M. Dubois, R. Frigot, P. Jardin, C. Leboucher, L. Maunoury, C. Seiffert, J. C. Thomas, and E. Traykov, *Phys. Rev. C* **91**, 032501(R) (2015).
- [40] M. Brodeur, J. Kelly, J. Long, C. Nicoloff, and B. Schultz, *Nucl. Instrum. Methods Phys. Res., Sect. B* **376**, 281 (2016).
- [41] D. Burdette, M. Brodeur, P. O'Malley, and A. Valverde, *Hyperfine Interact.* **240**, 70 (2019).
- [42] A. A. Valverde, M. Brodeur, D. P. Burdette, J. A. Clark, J. W. Klimes, D. Lascar, P. D. O'Malley, R. Ringle, G. Savard, and V. Varentsov, *Hyperfine Interact.* **240**, 38 (2019).